Residence time distribution measurements in an external-loop airlift reactor: Study of the hydrodynamics of the liquid circulation induced by the hydrogen bubbles

Abdel Hafid Essadki, Bouchaib Gourich, Christophe Vial, Henri Delmas

Residence time distribution measurements in an external-loop airlift reactor: Study of the hydrodynamics of the liquid circulation induced by the hydrogen bubbles

A.H. Essadki [a,*], B. Gourich [a], Ch. Vial [b], H. Delmas [c]

[a] Laboratoire d'Ingénierie de Procédés et d'Environnement, Ecole Supérieure de Technologie de Casablanca, BP 8012, Oasis Casablanca, Morocco
[b] Polytech'Clermont-Ferrand—LGCB, Bât. Polytech, 24 avenue de Landais, BP 206, 63174 AUBIERE Cedex, France
[c] Laboratoire de Génie Chimique, ENSIACET-INPT, 5 rue Paulin Talabot, 31106 Toulouse, France.

A B S T R A C T

A detailed study of the residence time distribution (RTD) analysis of liquid phase has been performed in an external-loop airlift reactor of 20 L nominal volume, regarded as a global unit and discriminating its different sections (riser, gas–liquid separator and downcomer) using the tracer response technique. The reactor was used as an electrochemical reactor in order to carry out the electrocoagulation/electroflotation (EC/EF). The gas phase created in the riser is the hydrogen produced by water electrolysis.

In order to use this reactor for a continuous EC/EF, hydrodynamic studies were carried out to control the operating conditions and to help modelling the electrocoagulation. Current density, position of the electrodes in the riser and the volumetric liquid flow (inlet flow) are the key parameters for the hydrodynamics.

The experimental results revealed that both in the downcomer and the riser–separator zones, the flow model is axial dispersion. Interesting results were obtained:

- The superficial liquid velocity (U_{Ld}) at the downcomer, decreased when the volume inlet flow increased ($0 < Q_L < 2$ L/min).
- The Peclet number obtained in the downcomer was correlated to the current density and the electrodes position.
- In the riser–separator zone the Peclet number decreased with the superficial liquid velocity in the riser indicating that the dispersion increased with an increase of turbulence created in the separator by an increase of liquid velocity.
- The percentage of flow that quits the reactor without reacting increased when the main flow increased and the current intensity decreased. The global RTD can be reconstituted by the signal resulting from the junction and that from riser–separator and downcomer zone by using the convolution technique. The experimental results confirm this reconstitution. The experiments confirm also that the liquid crosses the reactor without achieving loops in the case of the continuous flow.

1. Introduction

In general, residence time distribution (RTD) measurements are obtained from tracer experiments that consist of an impulse-response method. The injection of a tracer is done at the inlet of a system and a probe is introduced at the outlet to record the concentration–time curve. A variety of methods for the exploitation of experimental RTD is listed by Björnstad et al. (2001). RTD measurements constitute an efficient tool that can help better understand and determine different hydrodynamic parameters. The parameters identified allow for the modelling of many processes.

The importance of the study of residence time distribution (RTD) was proven to many chemical processes (Le Prince, 1998), concerning the design and the control of the process. In general, flow models are chosen to describe the fluid-dynamic behaviour of the system.

Several techniques were proposed to study the RTD measurements in different reactors as bubble column, packed bed, fluidized bed, internal-loop airlift and external-loop airlift reactors. The tracing of the liquid phase could be carried out by various methods. The most important measurements depend on

* Corresponding author. Tel: +212(0)6 60878671; fax: +212(0)5 22252245.
E-mail address: essadki@est-uh2c.ac.ma (A.H. Essadki).

the nature of the tracer concerning its conductivity, absorbance, phosphorescence, optical characteristics, etc. The measurements concern also the temperature and radiation.

The tracing by conductivity measurement is simple and allows for an efficient measurement with a basic conductimeter.

In concentric-tube airlift reactor, Gavrilescu and Tudose (1999), have studied RTD for different sections of the reactor (riser, downcomer, bottom zone and gas–liquid separator) and also for the whole reactor. The reactor was operated in biphasic continuous flow of liquid and gaseous phase. Other studies have studied the hydrodynamics of fluid in external-loop airlift reactor. Dhaouadi et al. (1996, 1997) found that the liquid flow in the riser and the downcomer was represented as plug flow with axial dispersion, while the gas–liquid separator and the bottom junction were considered as tank-in-series reactors for the liquid.

Vial et al. (2005) proposed a model predicting the axial dispersion coefficient in the riser of an external-loop airlift reactor. It used a turbulent diffusion coefficient to estimate the influence of two-phase turbulence on mixing.

The axial dispersion model was applied by Zhang et al. (2005) to the riser and downcomer of an airlift loop reactor.

Most applications of external-loop airlift reactors (EL-ALRs) concern chemical and biological processes. Recent studies concerning electrocoagulation/electroflotation in EL-ALRs are considered as innovative applications. Thus, in previous works, Essadki et al. (2008) used EL-ALRs to investigate decolourisation. The same external-loop airlift reactor was used first to investigate defluoridation of drinking water by EF/EF (Bennajah et al., 2009), and then in a comparative study in which the removal yield in an ELALR was compared to that at a stirred tank reactor (STR) (Essadki et al., 2009). These works highlighted that the EL-ALR did not require additional mechanical power for mixing, as this was induced only by the electrogenerated gas phase. Flotation was complete in the EL-ALR because the sludge was less eroded by mechanical stirring and could be recovered more rapidly than in a STR in which recovery had to be achieved both by flotation and settling.

The objective of this work is to determine the hydrodynamic behaviour in different sections of the EL-ALR by identifying different parameters needed for the modelling in order to predict the concentration profile in the exit of the reactor. Thus, the airlift reactor can be used for a continuous process (EC/EF) and the water will be treated without needing filtration.

In our case, the liquid flow is induced electrochemically. In fact the overall liquid circulation (flow) is induced by H_2 microbubbles generated by water electrolysis, contrary to the conventional EL-ALRs in which the driving force is due to the sparged gas introduced pneumatically. In addition, bubble sizes in electroflotation always fall in the range 20–70 μm (Adhoum et al., 2004), far smaller than those observed in conventional air assisted flotation, which provides both sufficient surface area for gas–liquid–solid interfaces and mixing efficiency to favour the aggregation of tiny destabilised particles. Hydrogen bubbles, which obey usually to a lognormal size distribution, are known to be the smallest about neutral pH (Murphy et al., 1992).

No work concerning RTD measurements was done in EL-ALRs functioning as electrochemical reactor, as far as the authors know.

2. Materials and methods

2.1. Reactor design

An external-loop airlift made of transparent Plexiglas was used for this study. The reactor geometry is illustrated by Fig. 1. The diameters of the riser and the downcomer are, respectively, 94 and 50 mm. Consequently, the riser-to-downcomer cross-sectional ratio (A_r/A_d) is about 3.5. This is a typical value when reaction takes place only in the riser section. Both riser and downcomer are 147 cm height (H_2+H_3) and are connected at the bottom by a junction of 50 mm diameter and at the top by a rectangular gas separator of H_S=20 cm height. The distance between the vertical axes of the riser and the downcomer is 675 mm, which limits the recirculation of bubbles/particles from the riser into the downcomer. The liquid volume is 20 L. The clear liquid height (h) corresponds to 14 cm in the separator section. All the experiments were conducted at room temperature (20 ± 1 °C) and atmospheric pressure in batch mode (reactor closed to the liquid phase) and in a continuous mode (reactor opened to the liquid phase). Contrary to conventional operation in airlift reactors, no gas phase was sparged at the bottom in the riser. Only electrolytic gases induced the overall liquid circulation (flow) resulting from the density difference between the fluids in the riser and the downcomer. Two readily available aluminium flat electrodes of rectangular shape (250 mm × 70 mm × 1 mm) were used as the anode and the cathode. The distance between electrodes was e=20 mm, which is a typical value in EC cells. The electrodes were placed in the riser, parallel to the main flow direction. The axial position of the electrode could also be varied in the column. The distance (H_1) between the bottom of the electrodes and the bottom of the riser ranged between 7 and 77 cm (Fig. 1). An intensiostat used a digital DC power supply (Didalab, France) to create electrolysis.

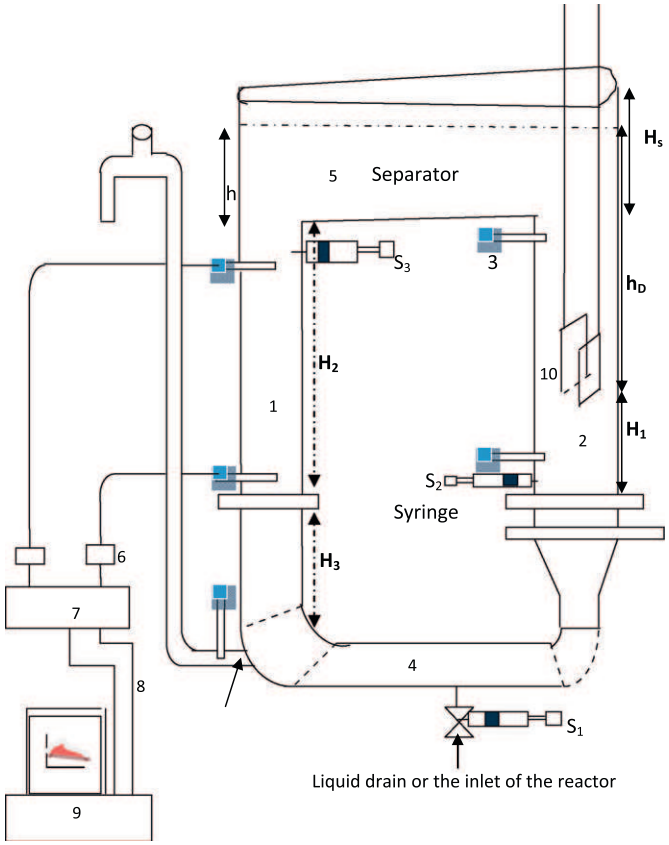

Fig. 1. External-loop airlift reactor (1: downcomer section; 2: riser section; 3: conductivity probes; 4: junction column; 5: separator; 6: conductimeter; 7: analogue output/input terminal panel (Omega OMB-55 acquisition system); 8: 50-way ribbon cable kit; 9: data acquisition system; 10: electrodes).

The main reactions during electrolysis are

$$\text{Anode}: \quad Al^0_{(s)} \rightarrow Al^{3+} + 3e^-$$

$$\text{Cathode}: \quad 2H_2O + 2e^- \rightarrow H_{2(g)} + 2OH^-$$

When pH is between 4 and 9, the Al^{3+} and OH^- ions generated by the electrodes react to form various monomeric species such as $Al(OH)_2^+$, $Al_2(OH)_2^{2+}$, and polymeric species such as $Al_6(OH)_{15}{}^{3+}$, $Al_7(OH)_{17}{}^{4+}$, $Al_{13}(OH)_{34}{}^{5+}$ that finally transform into insoluble amorphous $Al(OH)_{3(s)}$ through complex polymerisation/precipitation kinetics (Bayramoglu et al., 2004).

Additionally, at high current density, other reactions may be encountered at the anode, as the oxygen formation at the anode:

$$4OH^- \rightarrow O_2 + 2H_2O + 2e^-$$

In our case, for j less than 34.3 mA/cm^2 (I=6 A), O_2 was not observed, but for I=7 A the bubbles from the anode were observed indicating the presence of O_2.

2.2. Chemicals and methods

The average liquid velocity in the downcomer (U_{Ld}) and RTD were measured using the conductivity tracer technique. Two conductivity probes placed in the downcomer section were used to record the tracer concentration resulting from the injection of 5 mL of a saturated NaCl solution at the top of the downcomer using a data acquisition system based on a PC computer equipped with Omega OMB-55 A/D converter. The distance between the probes was 90 cm (Fig. 1). Two conductivity probes were also placed at the riser section in order to study RTD in this region. Liquid velocity was estimated using the ratio of the mean transit time between the tracer peaks detected successively by the two electrodes and the distance between the probes. The superficial liquid velocity in the riser (U_{Lr}) was deduced from a mass balance on the liquid phase

$$U_{Lr} = \left(\frac{A_d}{A_r}\right) U_{Ld} \tag{1}$$

Solution conductivity and pH were measured using a CD810 conductimeter (Radiometer Analytical, France) and a ProfilLine pH197i pHmeter (WTW, Germany).

Current density values (j) between 5.7 and 34.3 mA/cm^2 were investigated, which corresponds to current (I=jS) in the range 1–6 A.

3. Methodology of the study of RTD in the EL-ALR

The global reactor could be considered as an assembly of interconnection of elementary modules. RTD analysis of liquid phase is investigated in different sections of the external-loop airlift reactor functioning as a batch reactor. Each compartment is considered as a sub-system in which the liquid crosses this element by its own inlet and exit. When the inlet flow is introduced, both the elementary modules and the global reactor were studied as systems.

The response of the global reactor is then discussed in terms of its relation to the different responses of the different modules constituting the whole reactor.

The liquid RTD was determined by means of the tracer response technique. An approximated δ-Dirac pulse of tracer solution (NaCl) was injected into the reactors at a certain time (t=0) and the outlet signal was detected by conductivity probe and recorded by Omega OMB-55 acquisition system. The tracer was injected as quickly as possible to obtain as closely as practical a δ-pulse of tracer at the inlet.

The sections studied were the downcomer, the riser–separator section and the global reactor. Models were tested to obtain the most appropriate hydrodynamic parameters for each section of the reactor by fitting these models and the experimental data. Optimisation by least square method has been used to identify the hydrodynamic parameters (mean residence time, Peclet number and number of tanks in cascade). For each studied compartment of the reactor, the tracer was used by a syringe in a location considered as the inlet of the sub-system. At the exit of each compartment a conductimetric probe was installed to take measurements on line.

The probe to measure conductivity was previously calibrated so the tracer concentration could be determined from the recorded conductivity profile.

The age distribution of fluid leaving a vessel is called residence time distribution (RTD) noted $E(t)$. When we introduce a tracer by δ-Dirac pulse into the stream of the flowing fluid at time t=0, the recorded concentration $C(t)$ describes also the age distribution.

The mean residence time τ is defined by the following equation:

$$\tau = \frac{\int_0^\infty t C_{\mathrm{NaCl}}(t)dt}{\int_0^\infty C_{\mathrm{NaCl}}(t)dt} \tag{2}$$

To obtain the $E(t)$ curve from the $C(t)$ curve, we divided $C(t)$ by the integral $\int_0^\infty C_{NaCl}(t)\mathrm{d}t$

$$E_{exp}(t) = \frac{C_{\mathrm{NaCl}}(t)}{\int_0^\infty C_{\mathrm{NaCl}}(t)dt} \tag{3}$$

The differential equation representing the axial dispersion of a tracer is

$$\frac{\partial C}{\partial t} = D\frac{\partial^2 C}{\partial z^2} - U\frac{\partial C}{\partial z} \tag{4}$$

The analytical solution of such an equation (Levenspiel, 1992) taking into account the boundary conditions i.e in z=0 and in the measured point z=L is expressed as

$$E(t) = \frac{1}{2}\sqrt{\frac{\mathrm{Pe}}{\pi\tau t}}\exp\left(-\frac{\mathrm{Pe}(\tau - t)^2}{4\tau t}\right) \tag{5}$$

in which $\mathrm{Pe}=U(L/D)$ is the Peclet number, D is the axial dispersion, U is the liquid velocity, L is the length of the considered column and τ is the mean residence time.

In the case of a tracer flowing in a real reactor represented by the tank-in-series modelled by N reactors perfectly mixed, the mean residence time of each reactor is

$$\tau_1 = \tau_2 = \cdots = \tau_k = \cdots = \tau_N = \frac{\tau}{N} \tag{6}$$

$$\tau = \frac{V_R}{Q} \tag{7}$$

V_R is the volume of the reactor, Q the volumetric flow and τ the residence time of the real reactor.

For the kth reactor, the mass balance is

$$QC_{k-1} = QC_k + \frac{V_R}{N}\frac{dC_k}{dt} \tag{8}$$

The solution giving $E(t)$ curve is

$$E(t) = \left(\frac{N}{\tau}\right)^j \frac{t^{N-1}}{(N-1)!}\exp\left(-N\frac{t}{\tau}\right) \tag{9}$$

The tank-in-series model include both a piston reactor ($N \rightarrow \infty$) and a perfect mixed reactor (N=1).

Experimental data were fitted to the proposed models using a direct method (simplex) in order to obtain the unknown model parameters. MATLAB 7 (The Mathworks, USA) was chosen as the programming language. MS Excel was also used and least square method was also used in the Excel.

4. RTD curves corrections

To obtain more precise values of the parameters of the models, it is necessary to evaluate the errors related to the injection mode. The inputs were treated as perfect pulse inputs, although in practice it is impossible to obtain a perfect pulse. As the injection is not a real Dirac, the correction of the real curve $E(t)$ was improved by using two signals and by convolution–deconvolution method.

Both in the downcomer and in the riser sections two conductivities probes were used. The approximated δ-Diract injection was done in the top of the downcomer close to the first probe by using syringe S_3. The inlet signal is recorded by the first probe and the outlet signal by the second probe. For the riser, the approximated δ-Dirac injection was done in the bottom (syringe S_2) of the riser close to the first probe that recorded the inlet signal and the outlet signal was recorded by the second probe.

The time-dependent concentration of a tracer at the outlet of a section $s(t)$ can be described as the convolution of the concentration distribution at the inlet $e(t)$ with the theoretical residence time distribution $E(t)$:

$$s(t) = e(t) \times E(t) \tag{10}$$

Fast Fourier Transform (FFT) could be used to obtain $E(t)$ because the convolution becomes a simple product:

$$\mathrm{FFT}(s(t)) = \mathrm{FFT}(e(t)E(t)) = \mathrm{FFT}(e(t))\mathrm{FFT}(E(t)) \tag{11}$$

So,

$$\mathrm{FFT}(E(t)) = \frac{\mathrm{FFT}(s(t))}{\mathrm{FFT}(e(t))} \tag{12}$$

The inverse FFT (IFFT) function of the product leads to a deconvolution of $E(t)$:

$$\mathrm{IFFT}(\mathrm{FFT}(E(t))) = \mathrm{IFFT}\left(\frac{\mathrm{FFT}(s(t))}{\mathrm{FFT}(e(t))}\right) \tag{13}$$

From where the output which the system should have if it was subjected to a true impulse of Dirac:

$$E(t) = \mathrm{IFFT}\left(\frac{\mathrm{FFT}(s(t))}{\mathrm{FFT}(e(t))}\right) \tag{14}$$

Thus, we could identify all the parameters with a good estimation by fitting the models on $E(t)$ instead of $s(t)$.

5. Results and discussion

5.1. Downcomer compartment

Fig. 2 shows the influence of both the current intensity and position of the electrodes on the RTD. No inlet flow is introduced, the reactor is considered as a batch reactor.

All curves indicate that they are almost Gaussian and symmetrical about the mean residence time corresponding to the maximum of $E(t)$.

The mean fluid residence time is lower for $H_1=7$ cm corresponding to a location in which the position of the electrode corresponds to the bottom of the riser than for $H_1=47$ cm in which the electrodes occupy the middle position of the riser. When the current intensity (or current density) increases, the mean residence time decreases. In fact, the influence of the two parameters (position of electrodes and current density) can be replaced by the downcomer liquid superficial velocity (U_{Ld}) as one parameter. Thus, in a previous work (Essadki et al., 2008), U_{Ld} was

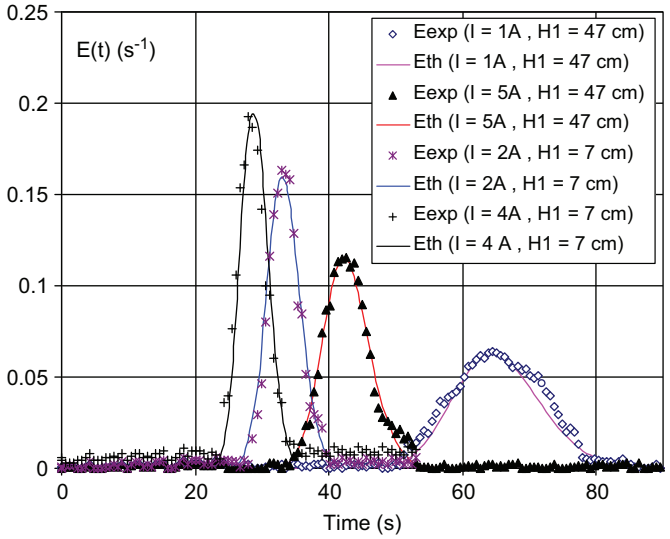

Fig. 2. E-curves in downcomer section (external-loop airlift as a batch reactor) for different current intensities and electrodes position. $Q_L=0$.

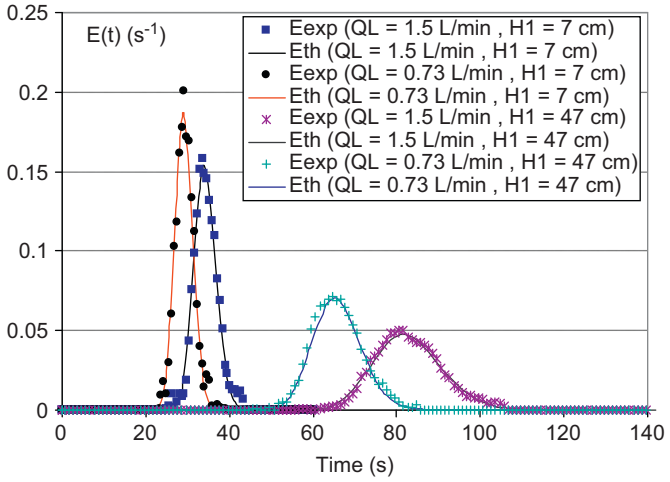

Fig. 3. E-curves in downcomer section (external-loop airlift as a continuous reactor) for different electrodes position and inlet flow-rate, $I=2$ A ($j=11.4$ mA/cm^2).

correlated by the following expression:

$$U_{Ld} = 5.8\left(\frac{h_D}{h_{D,max}}\right)j^{0.2} \tag{15}$$

Eq. (15) is of utmost importance for scale-up purpose at constant ratio (A_r/A_d). Nevertheless, if A_r/A_d had to be varied, one can benefit from the available know-how on external-loop airlift reactors to account for this effect (Joshi et al., 1990).

The inlet flow (the inlet of the rector in Fig. 1) is then introduced in El-ALR as a continuous reactor. Fig. 3 shows the influence of this parameter. It can be seen that the increase of the inlet flow-rate Q_L allows for an increase of the delay of the exit tracer. The current density was fixed at 11.4 mA/cm^2 ($I=2$ A).

The liquid flow-rate Q_{Ld} in the downcomer was measured by varying the inlet flow-rate Q_L.

$Q_{Ld}=U_{Ld}A_d$. The results of Q_{Ld} measurement versus Q_L are shown in Fig. 4. This figure indicates that Q_{Ld} decreases when Q_L increases for a fixed current intensity.

To explain this effect, we have to consider that, in airlift reactors, the driving force of the overall liquid circulation results

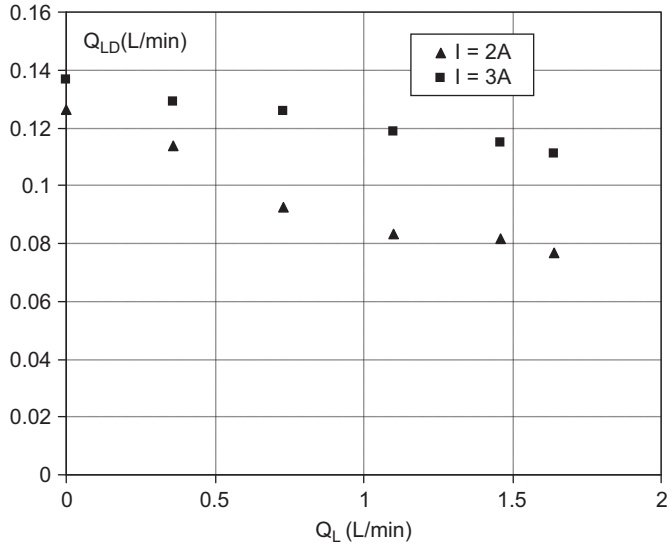

Fig. 4. Influence of the inlet flow-rate on the flow-rate in the downcomer (or riser) section for two current intensities, $H_1=47$ cm.

from the gas hold-up difference between the riser (ε_{Gr}) and the downcomer (ε_{Gd}), and also from the dispersion height.

The superficial liquid velocity in the riser U_{Lr} can therefore be predicted from an energy balance using the following equation (Chisti, 1989):

$$U_{Lr}=\sqrt{\frac{2gh_D(\varepsilon_{Gr}-\varepsilon_{Gd})}{K_T/(1-\varepsilon_{Gr})^2+(A_r/A_d)^2K_B/(1-\varepsilon_{Gd})^2}} \tag{16}$$

Dispersion height (h_D) corresponds to the distance from the surface in which a gas phase can be observed in the riser. In our case $\varepsilon_{Gd}=0$.

K_T is the coefficient expressing the effects of pressure drop in the riser and the separator section, K_B the coefficient expressing the effects of pressure drop in the downcomer and the junction.

In this work, the situation is however more complex because the gas phase is not injected, but electrochemically generated. This means that both h_D and ε_{Gr} depend on the axial position of the electrodes in the riser.

The introduction of an inlet flow increases the volume of the liquid in the riser section allowing for a decrease of the gas hold-up in this section, the velocity is then decreased as suggested by expression (16).

To analyse the experiment RTD data, a mathematical model has been selected. The best model representing the results is the axial dispersion model (piston flow+dispersion). Peclet number and the mean residence time were identified by fitting the experiment and mathematical model. In Fig. 5, Pe was plotted versus U_{Ld}. A linear tendency is observed and a correlation is found to be represented by the following expression:

$$Pe=35U_{\mathrm{Ld}}+25 \tag{17}$$

By replacing U_{Ld} by its expression (Eq. (15)), Pe number is then correlated to current density and dispersion height

$$Pe=203.7\left(\frac{h_D}{h_{D,max}}\right)j^{0.2}+25.1 \tag{18}$$

The mean residence time was also expressed versus U_{Ld} as indicated by Fig. 6. This figure shows that τ decreases when increasing U_{Ld}.

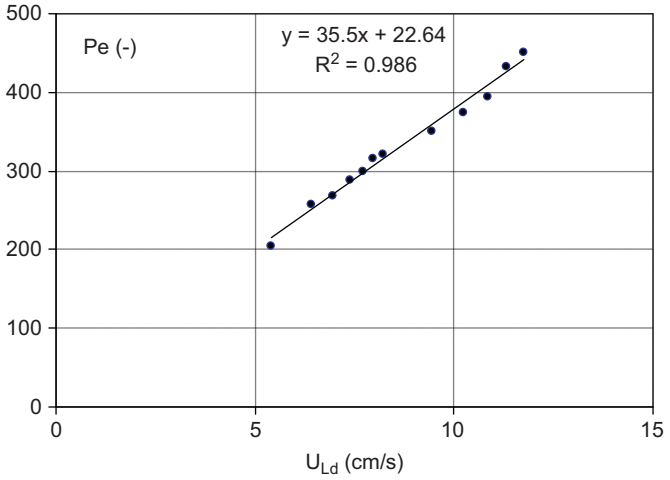

Fig. 5. Peclet (Pe) number versus the superficial liquid velocity in the downcomer section.

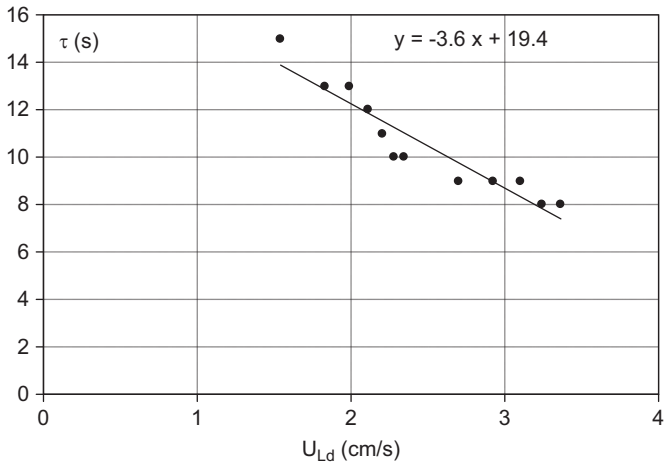

Fig. 6. Mean residence time versus the superficial liquid velocity in the downcomer section.

5.2. Riser–separator compartment

Because of the difficulty of realisation of RTD measurements in the separator, we have chosen to consider the riser and the separator together. The inlet (syringe S_3) of this sub-system is the bottom of the riser and the outlet is the top of the downcomer (conductimeter).

An example of the RTD measurement in this section is illustrated in Fig. 7 in which the symmetrical form disappeared. The model fitting well this part of reactor is tank-in-series model. In Fig. 7, the influence of both the position of the electrodes (H_1) and the inlet flow (Q_L) are shown. For $H_1=7$ cm and $Q_L=0.73$ L/min allowing for a superficial liquid velocity in the riser U_{Lr} of 2.85 cm/s ($U_{Ld}=10$ cm/s), the number of tanks in cascade N and mean residence time τ ($N=9$ and $\tau=121$ s) are lower than the case in which $H_1=47$ cm and $Q_L=0.36$ L/min allowing for a superficial liquid velocity in the riser of 1.9 cm/s ($U_{Ld}=6.6$ cm/s), $N=13$ and $\tau=204$ s.

The experiments revealed that in general, N is greater than 10, so the axial dispersion model (piston flow+dispersion) represents also the RTD experiments in this section. The parameter U_{Lr} influencing the hydrodynamic represents the influence of the two parameters (position of electrodes and current density). The experiments in this zone (riser+separator zone) showed that the increase of the riser superficial liquid velocity U_{Lr} between

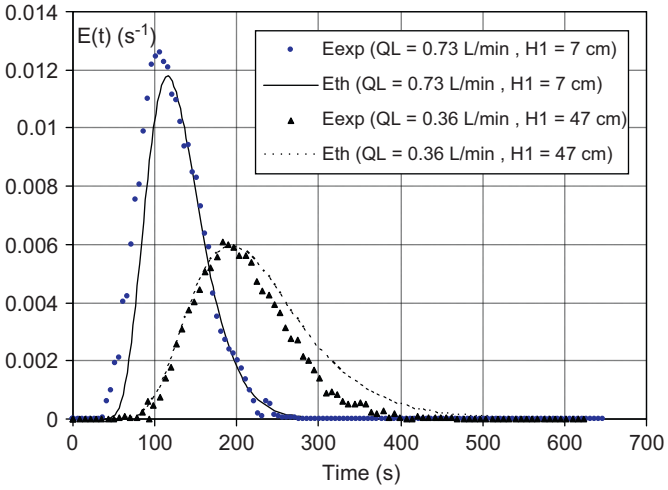

Fig. 7. *E*-curves in riser–separator section (external-loop airlift as a continuous reactor) for different electrodes position and inlet flow-rate. $I=3$ A ($j=17.1$ mA/cm^2).

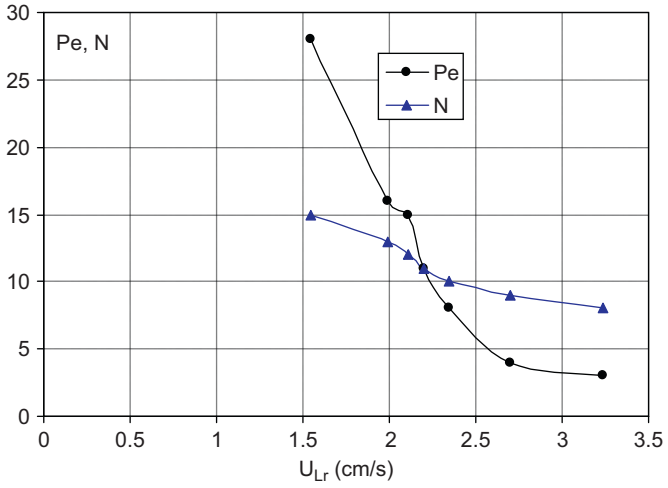

Fig. 8. Number of tanks-in-series for riser–separator section and the corresponding Peclet number versus the superficial liquid velocity in the riser section.

1.5 and 3.4 cm, induces a diminution of the number of tanks in cascade N from 15 to 8 corresponding to a decrease of Pe from 28 to 4. Fig. 8 shows that the number of tank-in-series or the Peclet number decreased when the superficial liquid velocity in the riser increased ($N=15$, Pe$=28$ for $U_{Lr}=1.5$ cm/s and $N=8$, Pe$=3$ for $U_{Lr}=3.5$ cm/s). It essentially shows that as the liquid velocity increases, the divergence from plug flow increases. This tendency is opposite to that in the downcomer in which Pe increases with liquid velocity. We can conclude that dispersion is favoured in the separation zone showing an increase in the turbulence intensity by an increase of liquid velocity. The mean residence time decreased from 250 to 113 s when U_{Lr} increased between 1.5 and 3.5 cm/s.

5.3. Global RTD

The reactor was operated in a continuous flow of liquid. The inlet volumetric liquid flow-rate Q_L varied between 0.1 and 2 L/min.

To get an optimal conductivity signal, the amount of tracer was increased. The syringe (S_1) was introduced in the drain that is open to the flow and represents the inlet of the whole reactor. The

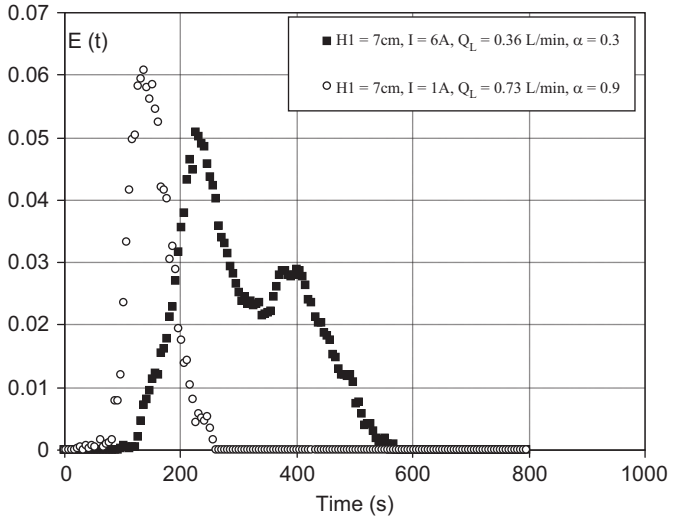

Fig. 9. *E*-curve as a global RTD in external-loop airlift reactor for ($Q_L=0.36$ L/min, $I=6$ A, $j=34.3$ mA/cm^2, $H_1=7$ cm, $\alpha=0.3$: 2 peaks) and ($Q_L=0.73$ L/min, $H_1=47$ cm, $I=1$ A, $j=5.7$ mA/cm^2, $\alpha=0.9$: 1 peak).

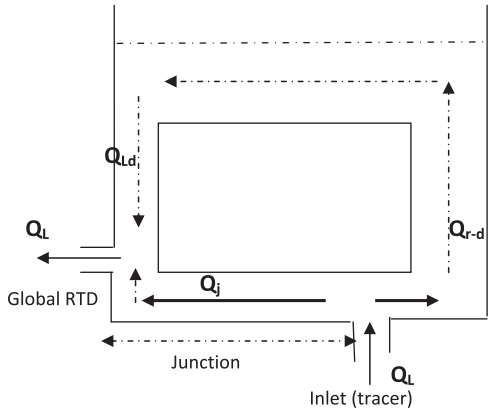

Fig. 10. Ways followed by the tracer inside the reactor: by the junction (αQ_L) and by the zone riser–separator and downcomer ($(1-\alpha)Q_L$).

probe conductivity was placed at the exit position of the reactor (Fig. 1). Examples of RTD measurements are shown in Fig. 9. Two kinds of signal are observed in this figure. One showed two peaks for the case of $Q_L=0.36$ L/min, $I=6$ A, $H_1=7$ cm and the other showed one peak for the case of $Q_L=0.73$ L/min, $I=1$ A, $H_1=47$ cm.

To analyse this behaviour, we have to consider Fig. 4. Thus, according to this figure, the flow-rate in the riser (Q_{rd}), equal to the flow-rate in the downcomer (Q_{Ld}), decreased when Q_L increased and for a fixed Q_L, Q_{Ld} (Q_{rd}) increased with the current intensity.

The main flow (Q_L) is divided into two flows: one exits directly the rector by crossing the junction (Q_j) and the other crosses the riser, the separator zone and the downcomer to exit the reactor (Q_{r-d}) as presented in Fig. 10.

$$Q_L = Q_i + Q_{r-d} \tag{19}$$

$$Q_L = \alpha Q_L + (1-\alpha)Q_L \tag{20}$$

$$Q_i = \alpha Q_L \text{ and } Q_{r-d} = Q_{Ld} = (1-\alpha)Q_L \tag{21}$$

Thus the global RTD can be described by the following expression:

$$E(t) = \alpha E_j(t) + (1-\alpha)E_{r-d} \tag{22}$$

E_{r-d} is the RTD representing the signal covering the riser, separator and the downcomer zones. This signal can be deduced by the convolution from the two signals resulting from the riser-separator zone and that from the downcomer

$$E_{r-d} = E_1(t) \times E_2(t) \tag{23}$$

in which $E_1(t)$ and $E_2(t)$ are, respectively, the downcomer and the riser–separator RTD. Both of them may be represented by the axial dispersion model (Eq. (5)).

By using FFT

$$\mathrm{FFT}(E_{r-d}) = \mathrm{FFT}(E_1)\mathrm{FFT}(E_2) \tag{24}$$

so,

$$E_{r-d} = \mathrm{IFFT}(\mathrm{FFT}(E_{r-d})) \tag{25}$$

The RTD representing the junction zone is also modelled by the axial dispersion model. The Peclet number is deduced by Eq. (17) by replacing U_{Ld} by the superficial liquid velocity in the junction column. The main residence time τ is estimated by dividing the length of this column by the superficial liquid velocity in the junction column.

For different values of Q_L and current intensity, α could be determined. Fig. 11 showed α versus Q_L for $I=2$ and 3 A. This figure shows that α increased with Q_L and decreased by increasing the current intensity. The second peak in Fig. 9 in which $\alpha=0.3$ can be explained. In fact the probe records two signals one coming directly by the junction, the other representing 70% of the tracer coming from the riser–separator and downcomer. For the case of $\alpha=0.9$, only 10% of the tracer crosses the zone riser–separator and downcomer to exit with a weak intensity of the signal.

A comparison between the experimental global E-curve and the theoretical E-curve (Eqs. from (22) to (25)) in the case of $I=1$ A, $Q_L=1.1$ L/min, $H_1=47$ cm is represented in Fig. 12 showing a good fit between the experiment and the model (Eqs. (22) and (23)). In this case $\alpha=0.85$, explaining one peak with a high intensity and another with low value.

6. Conclusion

The experimental RTD results showed that in downcomer, the flow model is axial dispersion. Both tank-in-series and axial dispersion models represent the riser–separator zone. The inlet flow decreased the velocity of the liquid in the downcomer.

The Peclet number (Pe) obtained for the downcomer was correlated to the current density and the electrodes position. Pe increased with the downcomer superficial liquid velocity.

In the riser–separation zone, the number of tanks decreased with superficial liquid velocity in the riser corresponding of a decrease of Pe (from 28 to 4). The tendency is opposite to that in the downcomer in which Pe increases with liquid velocity confirming that the dispersion is favoured in the separation zone, showing an increase in the turbulence intensity by an increase of liquid velocity.

The main flow (Q_L) is divided into two flows: one exit directly the rector by crossing the junction and the other crosses the riser, the separator zone and the downcomer to exit.

By taking into account this effect, the global RTD can be reconstituted by the signal resulting from the junction and that from riser–separator and downcomer zones. The experimental results confirm this reconstitution. The experiments confirm also that the liquid crosses the reactor without achieving loops in the case of the continuous flow.

The percentage of flow that quits immediately the reactor without reaction (riser compartment) increased when Q_L increased and the current intensity decreased.

So to support the reaction during the electrocoagulation, it is necessary to amplify the current intensity and to decrease the inlet flow. This is a disadvantage of this reactor functioning with continuous mode because the energy will increase and the amount of the treated pollutant decreases.

The goal of this work was focused on RTD measurements in an EL-ELAR functioning as an electrochemical reactor in which the gas (H_2) is electrochemically generated. The hydrodynamic parameters obtained could help modelling. This study enabled us to choose the parameters which can be useful in order to model the process. To increase the efficiency of EC in a continuous reactor, the mean residence time should be increased. The experiments showed that this effect is reached in the case of a relatively high value of current density and weak value of the inlet flow-rate. The position of the electrode should favour the electroflotation. In our case the best position is $H_1=47$ cm as suggested by the previous work (Essadki et al., 2009). This study highlights the hydrodynamic aspect of the flow in the external airlift reactor functioning

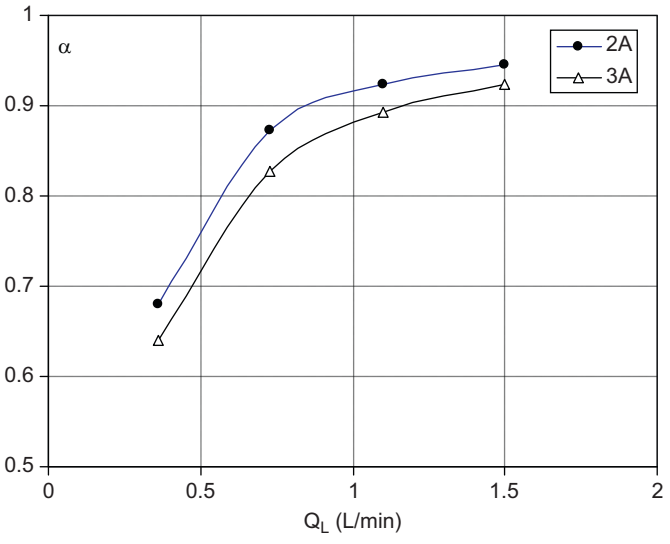

Fig. 11. Percentage of the flow (α) leaving the reactor by the junction versus the inlet flow-rate for two current intensities, $H_1=47$ cm.

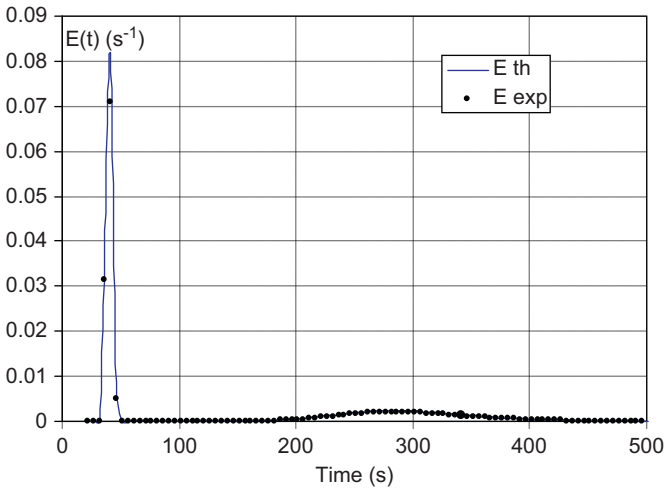

Fig. 12. Comparison between the experimental outlet E-curve (global) and E-curve resulting from the convolution of signals from association of connexion column, downcomer and riser–separator compartments: 1 A, 1.1 L/min, $H_1=47$ cm.

as a batch and continuous reactor and indicates that this arrangement is not suitable for continuous water treatment at high flow-rate; the design of this kind of reactor should be improved to allow the reactant to follow the compartment in which the reaction takes place (riser).

Nomenclature

A_d	cross-sectional area of the downcomer (m^2)
A_r	cross-sectional area of the riser (m^2)
e	electrode gap (m)
EC	electrocoagulation
EF	electroflotation
h	liquid height in the separator section (m)
h_D	dispersion height in Fig. 1 (m)
$h_{D,max}$	maximum dispersion height (m)
H_1	axial position of the electrodes in Fig. 1 (m)
H_2, H_3, H_S	geometrical characteristics of the reactor in Fig. 1 (m)
I	current (A)
j	current density (A/m^2)
K_B, K_T	friction factors in Eq. (6) (dimensionless)
L	electrode length (m)
N	number of tanks in cascades
Pe	Peclet number (dimensionless)
Q_L	inlet flow-rate (L/min)
Q_{Ld}	flow-rate in the downcomer section (L/min)
t	time (h)
τ	mean residence time (s)
U_{Gr}	superficial gas velocity in the riser (cm/s)
U_{Ld}	superficial liquid velocity in the downcomer (cm/s)
U_{Lr}	superficial liquid velocity in the riser (cm/s)
V_R	reactor volume (m^3)

Greek letters

ε_{Gd}	gas hold-up in the downcomer (dimensionless)
ε_{Gr}	gas hold-up in the riser (dimensionless)
α	percentage of flow in the junction

Reference

Adhoum, N., Monser, L., Bellakhal, N., Belgaied, J.-E., 2004. Treatment of electroplating wastewater containing Cu^{2+}, Zn^{2+} and Cr(VI) by electrocoagulation. Journal of Hazardous Materials 12, 207–213.

Bayramoglu, M., Kobya, M., Can, O.T., Sozbir, M., 2004. Operating cost analysis of electrocoagulation of textile dye wastewater. Separation and Purification Technology 37, 117–125.

Bennajah, M., Gourich, B., Essadki, A.H., Vial, Ch., Delmas, H., 2009. Defluoridation of Morocco drinking water by electrocoagulation/electroflottation in an electrochemical external-loop airlift reactor. Chemical Engineering Journal 148 (1), 122–131.

Björnstad, T., et al., 2001. Radiotracer Technology as Applied to Industry International Atomic Energy Agency IAEA-TECDOC. 1262 Vienna. pp. 2–11.

Chisti, Y., 1989. Airlift Bioreactors. Elsevier, London.

Dhaouadi, H., Poncin, S., Hornut, J.M., Wild, G., Oinas, P., 1996. Hydrodynamics of an airlift reactor: experiments and modeling. Chemical Engineering Scieqnce 51 (11), 2625–2630.

Dhaouadi, H., Poncin, S., Hornut, J.M., Wild, G., Oinas, P., Korpijarvi, J., 1997. Mass transfer in an extrernal-loopairlift reactor: experiments and modeling. Chemical Engineering Science 52 (21–22), 3909–3917.

Essadki, A.H., Bennajah, M., Gourich, B., Vial, Ch., Azzi, M., Delmas, H., 2008. Electrocoagulation/electroflotation in an external-loop airliftreactor—application to the decolorization of textile dye wastewater: a case study. Chemical Engineering and Processing 47, 1211–1223.

Essadki, A.H., Gourich, B., Vial, Ch., Delmas, H., Bennajah, M., 2009. Defluoridation of drinking water by electrocoagulation/electroflotation in a stirred tank reactor with a comparative performance to an external-loop airlift reactor. Journal of Hazardous Materials 168, 1325–1333.

Gavrilescu, M., Tudose, R.Z., 1999. Residence time distribution of the liquid phase in a concentric-tube airlift reactor. Chemical Engineering and Processing 38 (3), 225–238.

Joshi, J.B., Ranade, V.V., Gharat, S.D., Lele, S.S., 1990. Sparged loop reactors. Canadian Journal of Chemical Engineering 68, 705–741.

Le Prince, P., 1998. Procédés de Transformation. Editions Technip, Institut Français du Petrole, Paris, France.

Levenspiel, O., 1992. Chemical Reaction Engineering second ed. John Wiley and sons, Inc..

Murphy, O.J., Srinivasen, S., Conway, B.E., 1992. Electrochemistry in Transition: from the 20th to the 21st Century. Plenum, New York.

Vial, Ch., Poncin, S., Wild, G., Midoux, N., 2005. Experimental and theoretical analysis of axial dispersion in the liquid phase in external-loop airlift reactors. Chemical Engineering Science 60, 5945–5954.

Zhang, T., Wang, T., Wang, J., 2005. Mathematical modelling of the residence time distribution in loop reactors. Chemical Engineering and Processing 44, 1221–1227.